Journal of Alloys and Compounds, 186 (1992) 15–31
JALCOM 252

Calorimetric study of solid-state amorphization reaction of rod-milled Al_xTa_{1-x} alloy powders

M. Sherif El-Eskandarany, Kiyoshi Aoki and Kenji Suzuki
Institute for Materials Research, Tohoku University, Aoba-ku, Sendai 980 (Japan)

(Received September 9, 1991)

Abstract

In the present study, Al_xTa_{1-x} ($x=0.67$, 0.50 and 0.33) alloy powders have been prepared by mechanical alloying (MA) from pure powders of aluminium and tantalum using the rod-milling technique. Depending on the MA time and the aluminium content (x), various thermal properties of amorphization and crystallization are observed. The results can be summarized as follows: (1) At the intermediate stage of milling, heating the alloy powders to 700 K leads to the formation of an amorphous phase by the solid-state reaction. (2) The amorphization process occurs slowly in Al-rich alloy powders ($x=0.67$); however, in Ta-rich alloy powders, the amorphization process is fast. (3) The stability of the amorphous alloy powders presented by the crystallization temperature, T_x, increases as the aluminium content decreases. (4) The plot of the amorphous volume fraction *vs.* the MA time proves that the rate of the amorphization depends on one factor, *i.e.* the tantalum content in the alloy powders. It shows clearly that the rate of amorphization increases as this factor increases.

1. Introduction

The phenomenon of the solid-state amorphization reaction has received a great deal of attention since it was investigated by Schwarz and Johnson in 1983 [1]. A special type of solid-state reaction, called mechanical alloying (MA), was first discovered by Koch *et al.* [2] and used to produce Ni–Nb amorphous alloys using the ball-milling (BM) technique. So far, the BM technique has been used to prepare many amorphous alloy powders [3, 4] and metal nitrides [5, 6] at room temperature.

In 1990 El-Eskandarany *et al.* [7] reported another novel technique for preparing amorphous alloy powders by rod-milling (RM). MA [8, 9] and/or mechanical disordering (MD) [10] via the RM technique have been used successfully to produce many amorphous alloy powders such as Al–Nb [11] and Al–Zr [12] binary systems. More recently, the present authors have found that the rod-milled alloy powders of Al–TM (TM≡Ti, Zr, Nb and Ta) milled for about 86 to 360 ks of MA time transform to the amorphous state when heated in a differential thermal analyser [13, 14].

In this paper we report on calorimetric studies of the amorphization process for Al_xTa_{1-x} ($x=0.67$, 0.50 and 0.33) alloy powders produced by the MA process using the RM technique. The present work is an attempt to

0925-8388/92/$5.00

study the thermodynamics of the crystalline-to-amorphous transformation of the rod-milled Al_xTa_{1-x} alloy powders. We have also investigated the thermal stability of these alloys as a function of milling time. Further, we demonstrate how heating the rod-milled alloy powders leads to the formation of an amorphous phase by solid-state diffusion. One aim was to make a systematic study of a system for which there are very few thermodynamic data.

2. Experimental details

Pure elemental powders of aluminium (−325 mesh, 99.999%) and tantalum (−150 mesh, 99.99%) were mixed in a glove box under a purified argon atmosphere to give the desired average composition of $Al_{67}Ta_{33}$, $Al_{50}Ta_{50}$ and $Al_{33}Ta_{67}$. The MA process was performed by a cylindrical horizontal rotating stainless steel (SUS 304) rod-mill. The shell of the rod-mill was designed so that its length (250 mm) was greater than its diameter (120 mm) and the stainless steel (SUS 304) rods were cut to lengths (200 mm) less than the full length of the shell. The mixed powders were sealed in the rod-mill inside the glove box. In the present study, ten rods have been used as the milling media with 40 g of the powders.

The milling processing was carried out at ambient temperature by mounting the shell on a rotator which turned at the rate of 1.4 s^{-1}. The milling process was stopped periodically and the shell was opened in the glove box to take out about 1 g of the alloy powder as a sample for various analyses.

To follow the progress of the amorphization reaction, the rod-milled alloy powders were characterized by X-ray diffraction (XRD) using Mo Kα radiation, differential thermal analysis (DTA) under argon atmosphere at heating rate of 0.33 K s^{-1} and differential scanning calorimetry (DSC) in a flow of an argon gas (0.83 ml s^{-1}). All the DSC results presented in this paper were obtained with 0.67 K s^{-1}. However, some alloys were heated at several different heating rates to determine the amorphization activation energies. The metallography and the morphology of the alloy powders were studied by optical microscopy and transmission electron microscopy (TEM) using a 200 kV microscope. The samples for TEM observations were prepared by mounting the powders on a copper microgrid. Details of these experiments have been described in a previous paper [4].

3. Results

Figure 1 shows the XRD patterns of $Al_{67}Ta_{33}$ alloy powders as a function of the MA time. The XRD patterns of $Al_{33}Ta_{67}$ and $Al_{50}Ta_{50}$ alloy powders have been given in previous papers [7, 10]. At an early stage of MA time

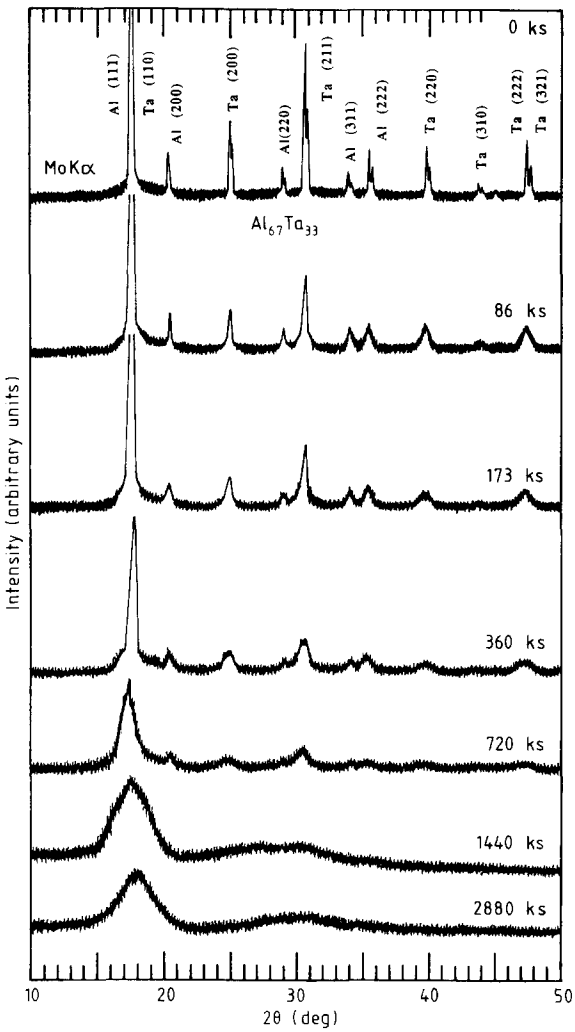

Fig. 1. XRD patterns of $Al_{67}Ta_{33}$ alloy powders as a function of the MA time.

(0–360 ks) the intensities of the Bragg peaks for pure aluminium and tantalum crystals decrease simultaneously with increase in milling time, as shown in Fig. 1. At the intermediate stage of MA (360–720 ks) almost all the minor Bragg peaks from elemental f.c.c. aluminium and b.c.c. tantalum crystals disappear. Further, the major Bragg peaks from pure Al (111) and Ta (110 and 211) reflections become wider, indicating the formation of an amorphous phase. At the final stage of MA (1440–2880 ks) a homogeneous amorphous phase is formed, characterized by broad haloes and smooth peaks.

Figure 2 shows the structure of the composite powder particles for $Al_{67}Ta_{33}$ alloy at the early stage of MA. After 43 ks of MA, the starting constituents of aluminium and tantalum are agglomerated as a result of the

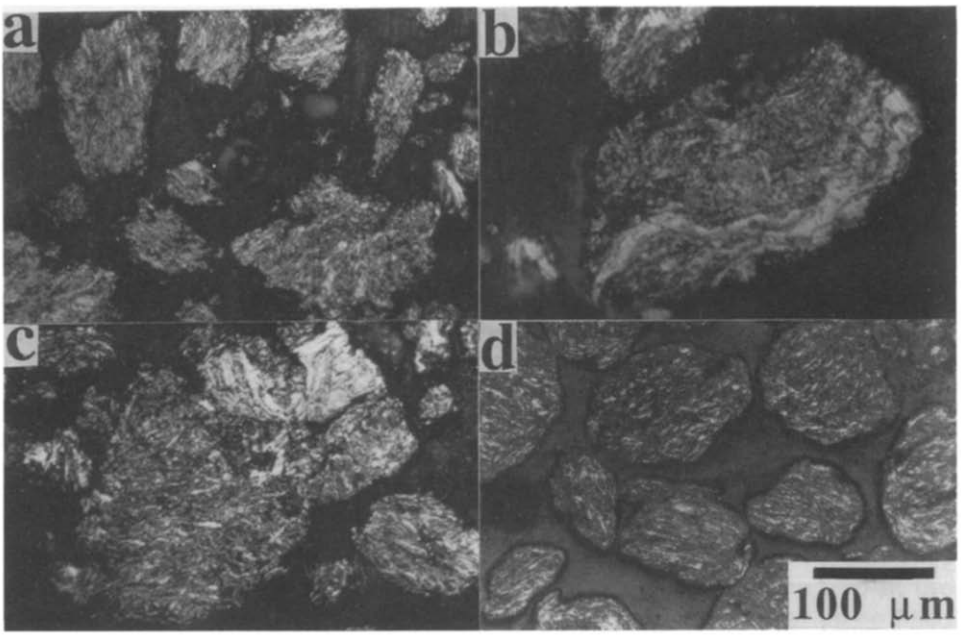

Fig. 2. Optical micrographs for polished powder particles of $Al_{67}Ta_{33}$ alloy after MA time of: (a) 43 ks; (b) 86 ks; (c) 173 ks; (d) 360 ks.

cold welding, as shown in Fig. 2(a). The composite particles tend to grow to form powder particles of greater diameter, as large as several hundred microns, as shown in Figs. 2(b) and 2(c). At this stage of milling, the particles are layered composites of the starting materials. Using an electron microscope analysis it was found that the white parts are aluminium layers and the dark parts are tantalum rich. The same observations for $Al_{33}Ta_{67}$ and $Al_{50}Ta_{50}$ are found elsewhere [8, 9].

Towards the end of the early stage of milling (360 ks) the particles have a well-aligned layered microstructure and individual layer width is reduced and becomes finer. Further, the size of the particle powders are reduced to be less than 100 μm in diameter, as shown in Fig. 2(d).

The DTA curves of $Al_{67}Ta_{33}$ alloy powders after different milling times are shown in Fig. 3. This figure shows that the MA process can be classified into three dependent stages: *i.e.* the early, intermediate and final stages of milling. During the early stage of MA (0–43 ks), the aluminium in the alloy powders melts, characterized by a sharp endothermic peak appearing at about 950 K. Then this melt reacts with the tantalum powders in the mixture of Al–Ta, characterized by a broad exothermic peak appearing at about 1200 K. The process at this stage is simply the blending of the two elemental metal powders [10]. After 86 ks of milling, both the endothermic and the high-temperature exothermic peaks disappear. Two broad exothermic peaks appear at about 550 K and 650 K. The temperature (peak temperature) of the first exothermic peak does not change with milling time and appears at

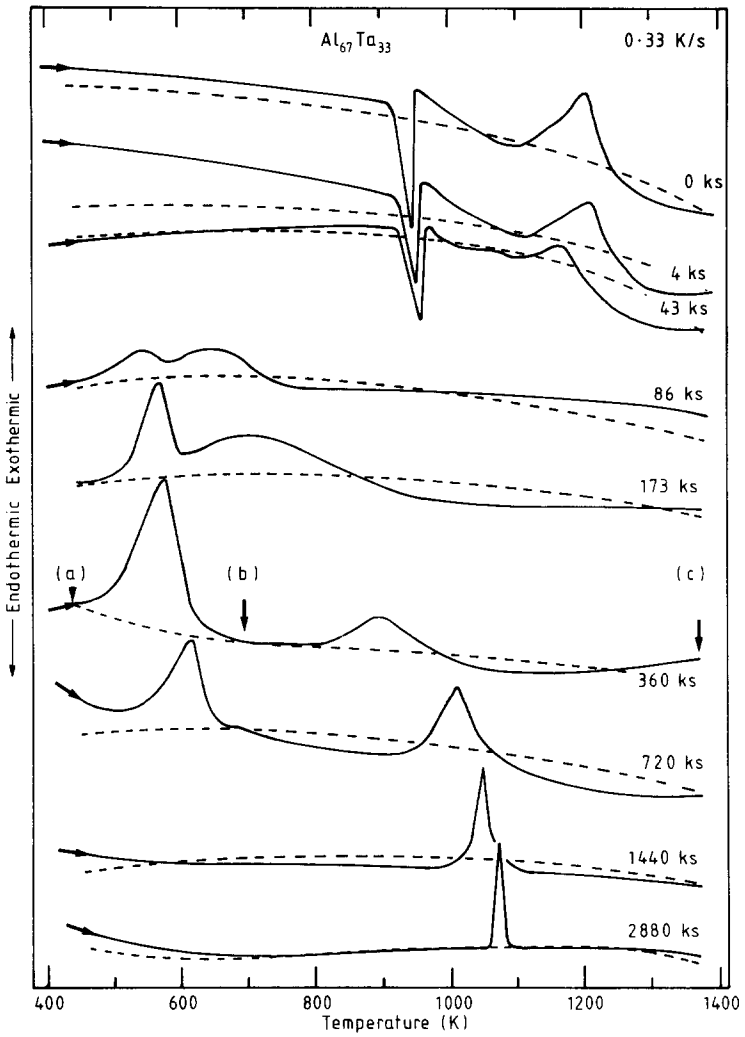

Fig. 3. DTA curves of $Al_{67}Ta_{33}$ alloy powders as a function of MA time.

about 600 K. In addition, this low-temperature exothermic peak disappears after 1440 ks of MA time. In contrast to this, the second exothermic peak is dependent on MA time in that it shifts to the elevated temperature and become sharp at the final stage of milling (1440–2880 ks), as illustrated in Fig. 3.

The TEM technique has been used to identify the origin of the two exothermic peaks, so that three samples were heated separately in the DTA at (a), (b) and (c), as shown in Fig. 3. The direct TEM imaging of the phase formation for these samples at 500 K (a), 700 K (b) and 1400 K (c) is shown in Fig. 4. The electron diffraction pattern from several regions of sample (a) show Debye–Scherrer rings that are characteristic of several

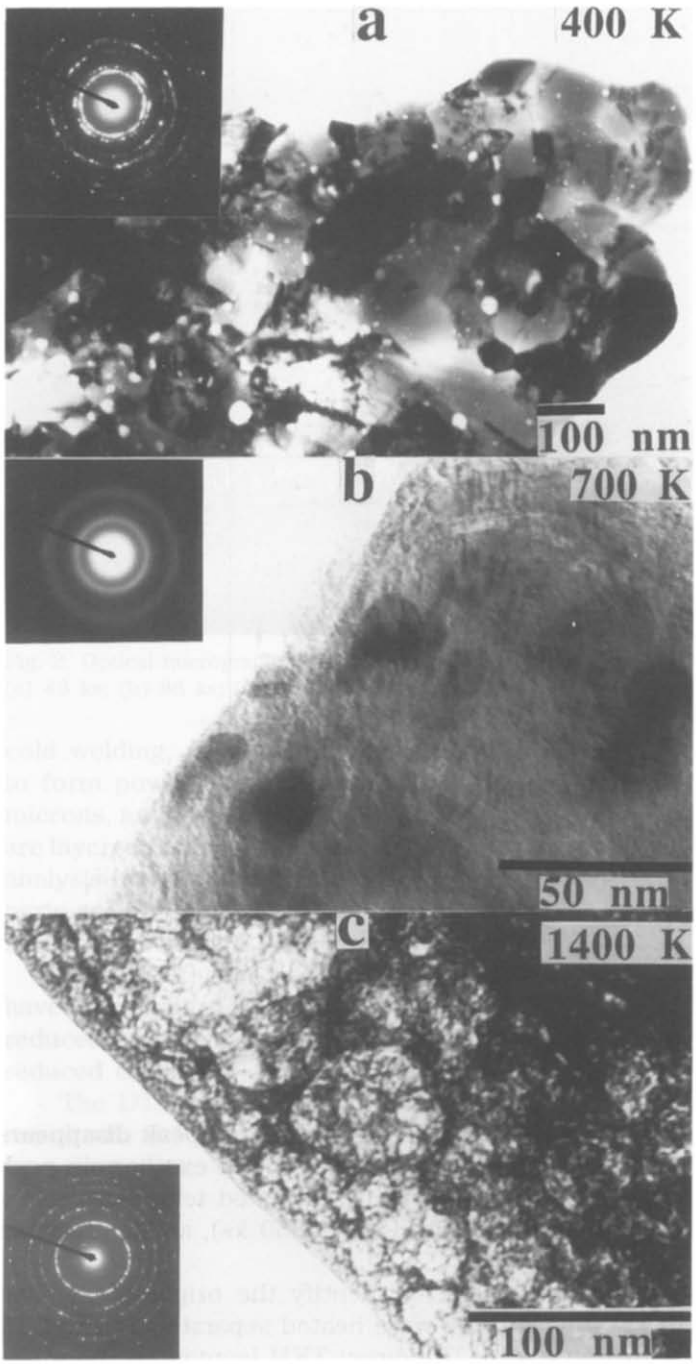

Fig. 4. The bright-field images and the corresponding diffraction patterns of $Al_{67}Ta_{33}$ alloy powders milled for 360 ks, then heated to: (a) 400 K; (b) 700 K; (c) 1400 K.

diffracting polycrystalline Al–Ta. In sample (b), however, the electron diffraction pattern indicates the formation of an amorphous phase, characterized by a clear visible halo pattern. In addition, the bright-field image of sample (b) shows a fine structure and no microstructure with the size 50 nm is observed. At 1400 K (sample (c)) the halo pattern is replaced with a sharp ring pattern resulting from the crystallization of the amorphous phase. Moreover, the bright-field image of sample (c) has a micrograin structure with the average size of about 40 nm.

Figure 5 illustrates the DSC curves of the low-temperature exothermic peak (amorphization peak) for $Al_{67}Ta_{33}$ (a), $Al_{50}Ta_{50}$ (b) and $Al_{33}Ta_{67}$ (c) as a function of MA time. DSC has been used to obtain the values of the amorphization temperature, T_a, and the enthalpy change of amorphization, ΔH_a, more accurately.

Figure 6 presents the temperature (peak temperature) of amorphization, T_a (a) and the crystallization temperature, T_x, (b) as a function of MA time. It is worth noting that the value of T_a for Al_xTa_{1-x} alloy powders is independent of MA time, which suggests that a thermal-assistance amorphization takes place. However, T_x increases monotonically with increasing MA time in the early and intermediate stages of milling, indicating a continuous change in the composition of the amorphous phase, as shown in Fig. 6(b). It is worth noting that after 1080 ks of MA time, the T_x values of $Al_{33}Ta_{67}$ and $Al_{50}Ta_{50}$ alloy powders approach saturation values of 1216 K and 1210 K respectively. On the other hand, the T_x of $Al_{67}Ta_{33}$ reaches a saturation value (1067 K) after 2160 ks of MA time.

The activation energy of amorphization reactions, E_a, for Al_xTa_{1-x} alloy powders was determined by the Kissinger method [15]. The E_a has been determined by the DSC measurements at heating rates of 0.083, 0.167, 0.333, 0.500 and 0.667 K s^{-1}. Figure 7 summarizes the results of the E_a for Al_xTa_{1-x} after 86 ks of MA time. In Fig. 7, Φ and T_p are the heating rate and the peak temperature respectively. The E_a values for $Al_{67}Ta_{33}$, $Al_{50}Ta_{50}$ and $Al_{33}Ta_{67}$ are calculated from the slope of the lines to be 274, 180 and 177 kJ mol^{-1} respectively. The E_a value does not change with a change in MA time.

Figure 8 shows the enthalpy change of amorphization, ΔH_a, for Al_xTa_{1-x} alloy powders as a function of the MA time. The value of ΔH_a decreases sharply during the first stage of the milling time and approaches minimum values of -5.42, -4.37 and -2.24 kJ mol^{-1} for $Al_{67}Ta_{33}$, $Al_{50}Ta_{50}$ and $Al_{33}Ta_{67}$ alloy powders respectively. The ΔH_a then increases with increasing milling time to be nil at the final stage of the MA time.

The enthalpy change of crystallization, ΔH_x, for Al_xTa_{1-x} alloy powders is shown as a function of the MA time in Fig. 9. The values of ΔH_x were calculated from the area under the single crystallization exothermic peaks which appeared during the DTA measurements. The ΔH_x values tend to decrease sharply during the early and the intermediate stages of milling. They then approach a saturation value of -43 kJ mol^{-1} and -46 kJ mol^{-1} after 1080 ks of MA time for $Al_{50}Ta_{50}$ and $Al_{33}Ta_{67}$ alloy powders respectively,

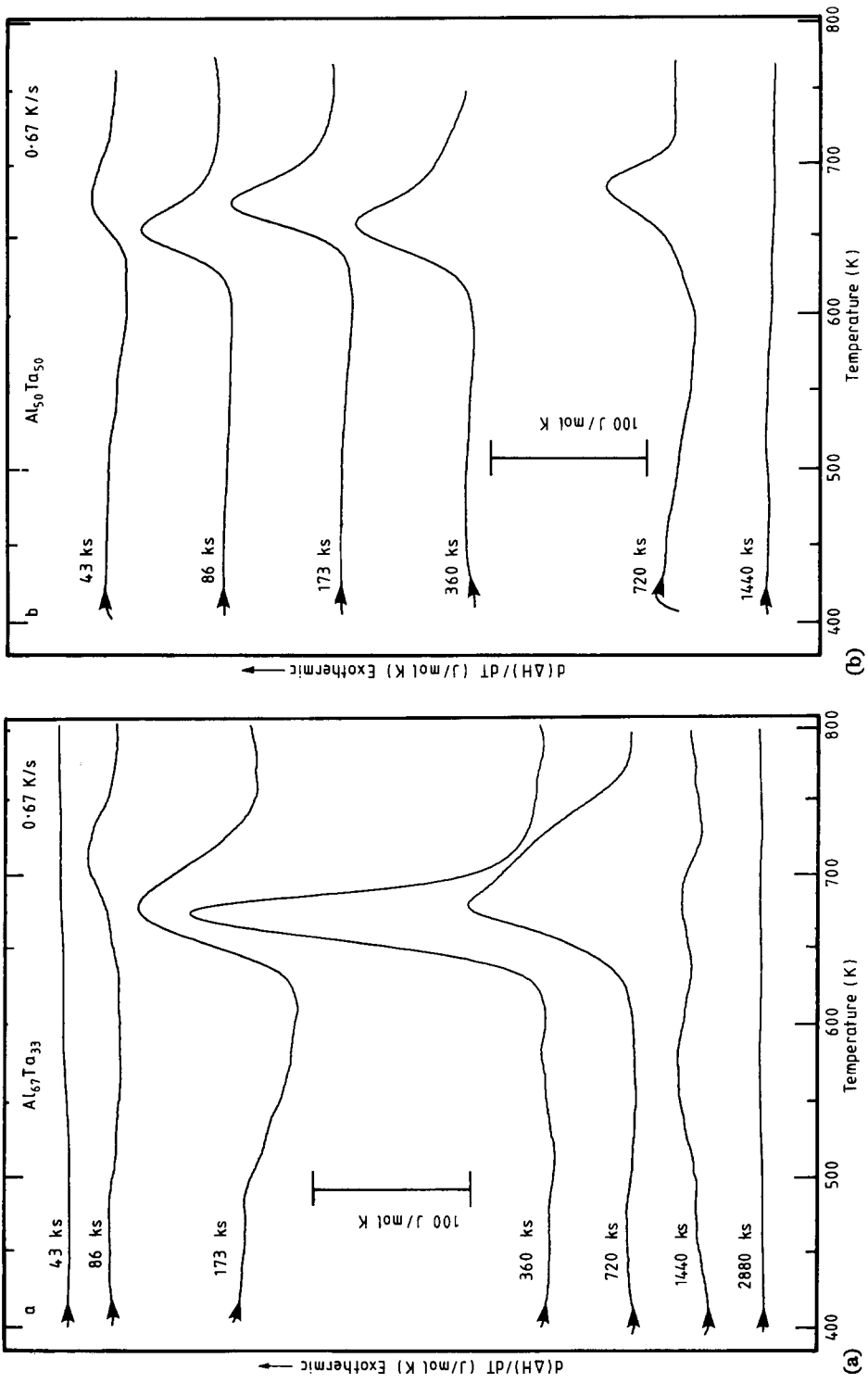
(a)
a
$Al_{67}Ta_{33}$
0·67 K/s
43 ks
86 ks
173 ks
360 ks
720 ks
1440 ks
2880 ks
100 J/mol K
d(ΔH)/dT (J/mol K) Exothermic
Temperature (K)
400
500
600
700
800
(b)
b
$Al_{50}Ta_{50}$
0·67 K/s
43 ks
86 ks
173 ks
360 ks
720 ks
1440 ks
100 J/mol K
d(ΔH)/dT (J/mol K) Exothermic
Temperature (K)
400
500
600
700
800

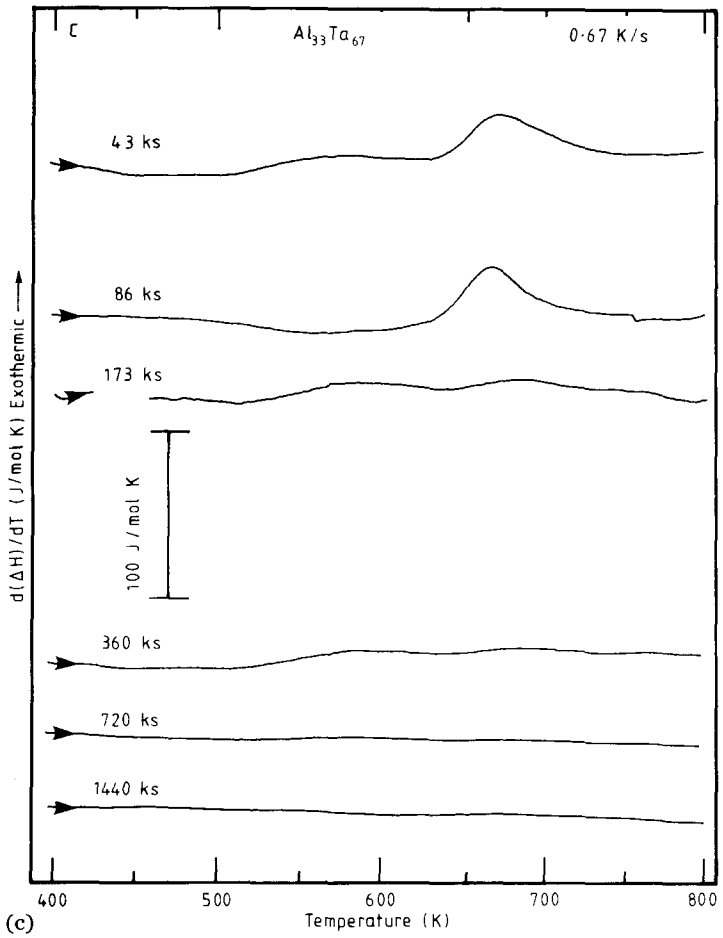

(c)

Fig. 5. DSC curves of the amorphization peaks for alloy powders as a function of MA time: (a) $Al_{67}Ta_{33}$; (b) $Al_{50}Ta_{50}$; (c) $Al_{33}Ta_{67}$.

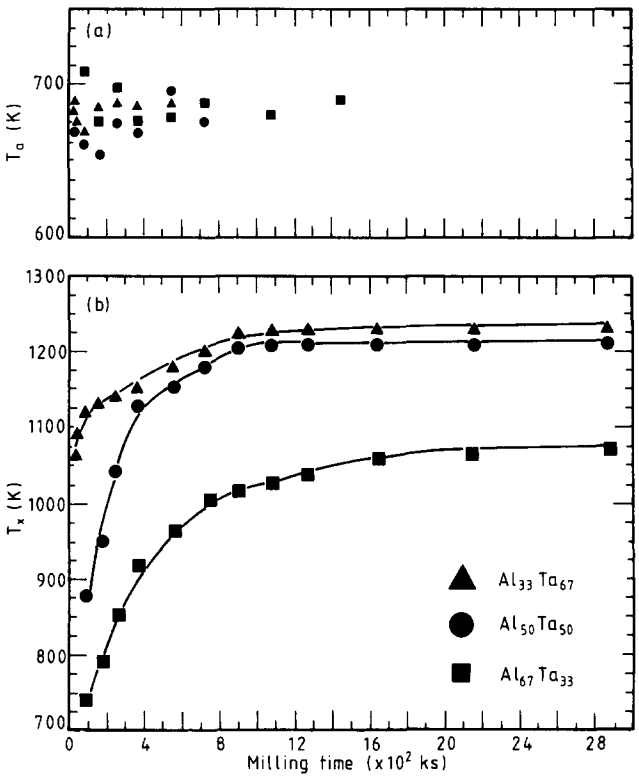

Fig. 6. Effect of MA time on amorphization and crystallization temperatures of Al_xTa_{1-x} alloy powders: (a) amorphization temperature, T_a; (b) crystallization temperature, T_x.

whereas, the ΔH_x values of $Al_{67}Ta_{33}$ alloy powders reach their saturation value of -34 kJ mol^{-1} after 2160 ks of MA time, as shown in Fig. 9.

In order to analyse the kinetic behaviour of amorphous–crystalline transition under MA, it is necessary to determine the amount of the amorphous phase with the MA time. According to the Johnson–Mehl–Avrami [16, 17] model of crystallization by nucleation and growth morphology, the relationship between the transformed volume fraction, x, and reaction time, t (in this work t is the MA time) is given as:

$$x = 1 - \exp[-(Kt)^n] \tag{1}$$

where K is a thermally activated rate constant and n is the Avrami exponent.

In this work, the amount of the amorphous phase at each milling time, x_t is determined in the following way:

$$x_t = \Delta H_{x_t} / \Delta H_{x_{max}} \tag{2}$$

where ΔH_{x_t} is the enthalpy of crystallization at the MA time, t and $\Delta H_{x_{max}}$ is the maximum value of crystallization enthalpy calculated from the DTA measurements at 2880 ks of MA time. The volume fraction of amorphous phase for Al_xTa_{1-x} alloy powders which is calculated from eqn. (2) is illustrated

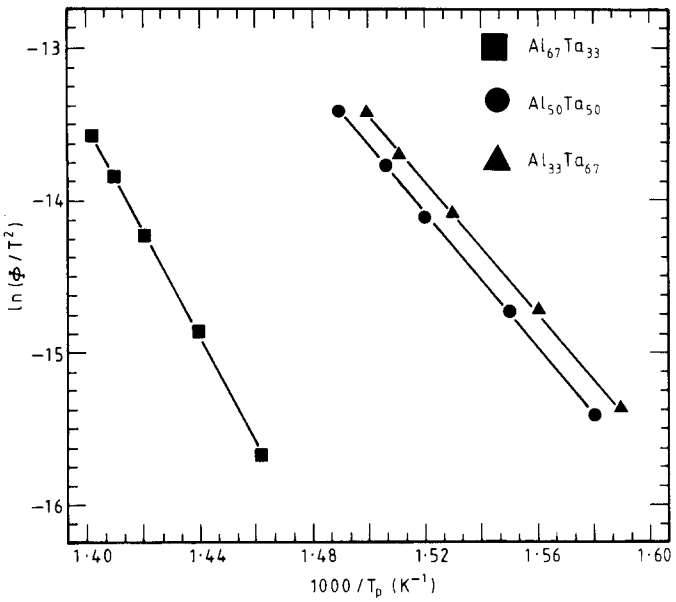

Fig. 7. Kissinger plot of the amorphization peak for Al_xTa_{1-x} alloy powders milled for 86 ks.

in Fig. 10. It shows clearly that the rate of amorphization increases with increasing tantalum content.

Figure 11 shows the Johnson–Mehl–Avrami plot for Al_xTa_{1-x} alloy powders. The values of the Avrami exponent, n, are determined from the slope of the straight lines to be 1.75, 1.11 and 0.34 for $Al_{67}Ta_{33}$, $Al_{50}Ta_{50}$ and $Al_{33}Ta_{67}$ respectively.

4. Discussion

On the basis of the evidence presented above it is clear that the MA process for producing Al_xTa_{1-x} amorphous alloy powders can be classified into three stages, *i.e.* agglomeration, amorphization and homogenization. At the agglomeration stage (0–360 ks), the powder particles of aluminium and tantalum are agglomerated as a result of the cold welding to appear of larger diameter, as large as several hundred microns. The optical microscopy observation of the cross-section of the particles reveals that they have a layered-structure morphology, as illustrated in Fig. 2. Moreover, the electron probe microanalysis (EPMA) shows that the powder particles vary widely in composition from one composite particle to another, indicating that the MA process takes place heterogeneously. In the amorphization stage of milling (360–720 ks) the size of the particles is reduced and the width of the layers becomes finer as a result of the continuous shear force which is generated by the rods. At the homogenization stage, the final stage of milling (720–2880 ks), the layered-structure morphology has already disappeared and the powder

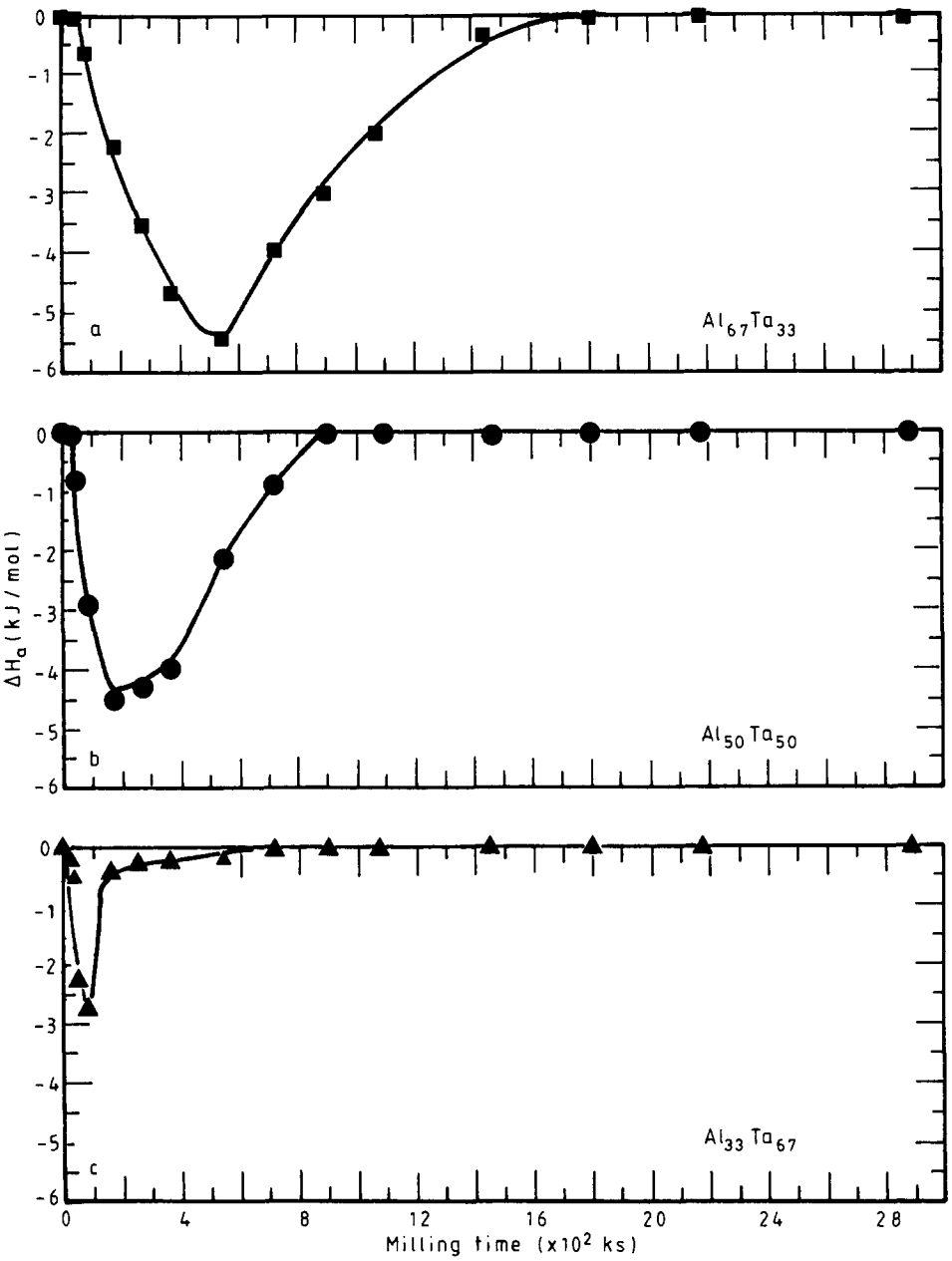

Fig. 8. The enthalpy change of amorphization, ΔH_a, for alloy powders as a function of MA time: (a) $Al_{67}Ta_{33}$; (b) $Al_{50}Ta_{50}$; (c) $Al_{33}Ta_{67}$.

particles become spherical with a size less than 1 μm in diameter. Moreover, the EPMA has shown that all the powder particles have the same composition, which suggests that the MA process occurs homogeneously.

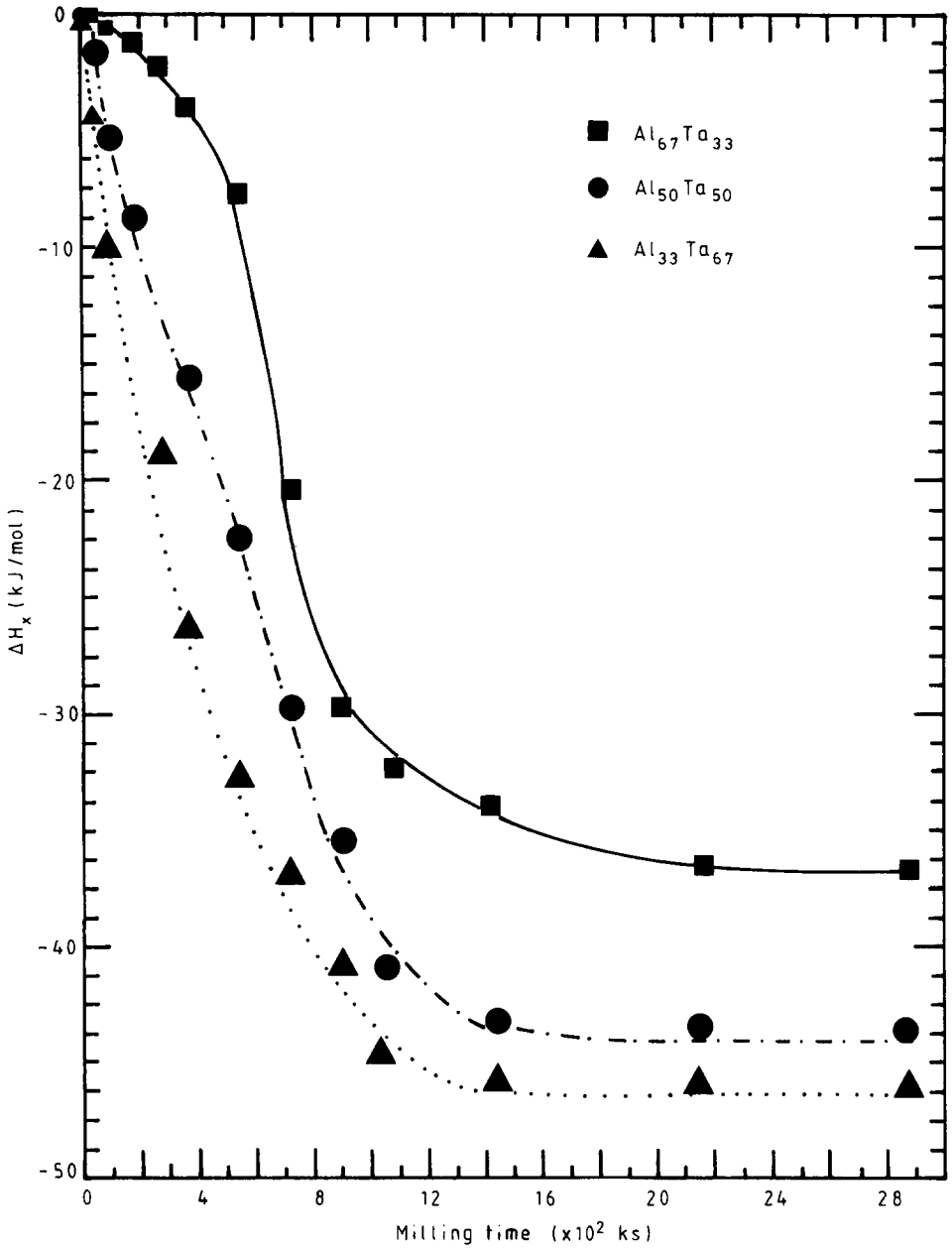

Fig. 9. The enthalpy change of crystallization, ΔH_x, for Al_xTa_{1-x} alloy powders as a function of the MA time.

At the early and the intermediate stages of milling, the DTA traces of Al_xTa_{1-x} alloy powders show two exothermic peaks, as shown in Fig. 3. The first exothermic peak appears at a relatively low temperature (around 650

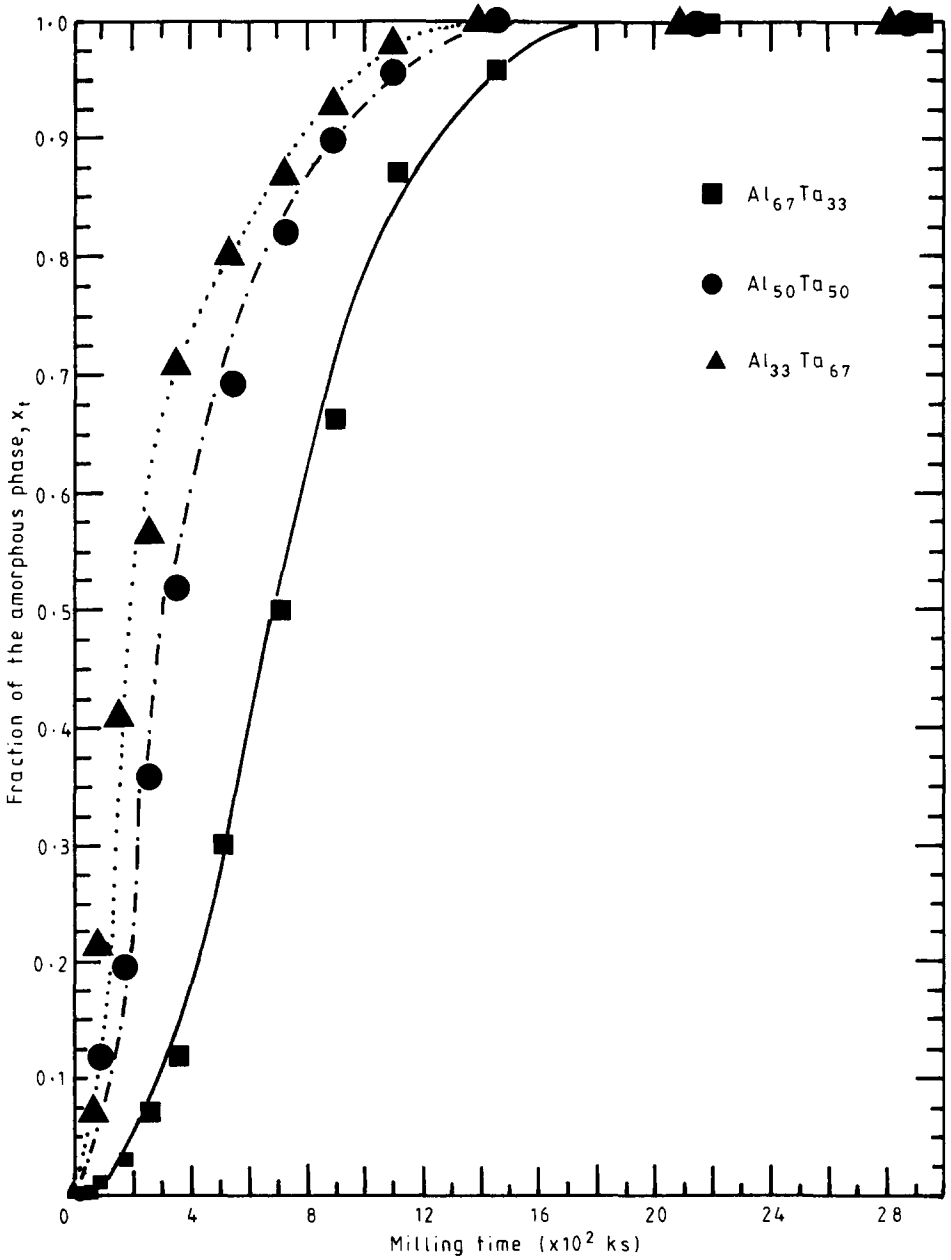

Fig. 10. The plot of the fraction of the amorphous phase in Al_xTa_{1-x} alloy powders *vs.* MA time. The fraction is calculated using eqn. (2).

K), while the second peak occurs at the elevated temperature. TEM imaging, which was carried out after each exothermic reaction has shown that the first exothermic peak is attributable to a solid-state amorphizing reaction

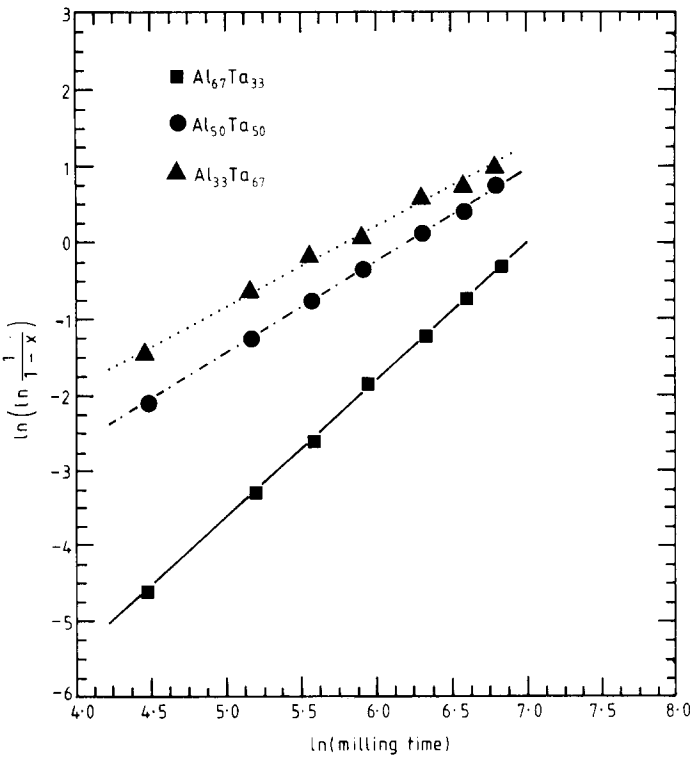

Fig. 11. The plot of $\ln(\ln 1/1-x_t)$ *vs.* ln(MA time), for Al_xTa_{1-x} alloy powders. x_t denotes the fraction of the amorphous phase in the milled powders.

between the fresh surfaces of aluminium and tantalum layers, as illustrated in Fig. 4. At the early stage of MA the XRD patterns of the rod-milled alloy powders did not show the formation of an amorphous phase (Fig. 1). Thus, the second exothermic peak occurs mainly as a result of the crystallization of the amorphous phase which was formed by the heating of the alloy powders during the DTA measurements. The $|\Delta H_a|$ of the Al_xTa_{1-x} increases sharply during this stage due to the appearance of the Al–Ta layers. At the amorphization stage of milling, however, the layer-structure morphology is scarcely detectable in most of the particles, but still appears in some of them. We should emphasize that the characteristic structure containing the aluminium and tantalum layers appears and then disappears quickly in the case of the $Al_{50}Ta_{50}$ and $Al_{33}Ta_{67}$ alloy powders. According to our results, it has been shown that the $Al_{67}Ta_{33}$ alloy has a high activation energy of amorphization, which may lead to a slow amorphization reaction. The lower the activation energy, the faster the amorphization reaction proceeds, as shown for $Al_{50}Ta_{50}$ and $Al_{33}Ta_{67}$ alloy powders. Therefore, the solid-state amorphizing reaction indicated by the $|\Delta H_a|$ for $Al_{50}Ta_{50}$ and $Al_{33}Ta_{67}$ alloy powders decreases sharply during this stage of milling and tends to zero after only 900 and 720 ks of milling respectively. In contrast, the $|\Delta H_a|$ for

$Al_{67}Ta_{33}$ decreases very slowly to be nil after 1800 ks of the MA time, as shown in Fig. 8. Moreover, the rate of amorphization depends on two factors, *i.e.* the milling time and the tantalum content in the alloy powders. The rate of amorphization increases as these two factors increase. In this study, the rate of amorphization is indicated by the fraction of the amorphous phase *vs.* the MA time using eqn. (2), as shown in Fig. 10.

At this stage of milling, the XRD patterns show the formation of an amorphous phase. It is worth remarking that this amorphous phase occurs mainly as a result of the further milling of the alloy powders. Moreover, the T_x and $|\Delta H_x|$ increases drastically, suggesting a rapid compositional change and an increase in the volume fraction of the amorphous phase respectively, as illustrated in Fig. 6.

At the homogeneous stage of milling, the layers of aluminium and tantalum in all the particles have already disappeared. Therefore, the first exothermic peak is absent, indicating the end of the amorphization reaction. In this stage of milling, the T_x and ΔH_x have approached to saturation values, reflecting the fact that the MA process occurs homogeneously.

5. Conclusion

This is a systematic study of the mode of amorphization process of $Al_{67}Ta_{33}$, $Al_{50}Ta_{50}$ and $Al_{33}Ta_{67}$ alloy powders produced by the mechanical alloying of the elemental powders of aluminium and tantalum using the rod-milling technique. The present study permits the following interpretations:

(1) The MA process is carried out through three dependent stages, *i.e.* early, intermediate and final stages.

(2) At the early stage of milling, the powder particles tend to grow in size to form powders of greater diameter, as large as several hundred microns. The cross-section of these particles shows a layer-structure morphology. This stage is followed by continuous disintegration until the size of the particles is less than 100 μm in diameter. At the final stage of milling, the particle size is less than 1 μm and the layer-structure has already disappeared.

(3) At the early and intermediate stages of rod-milling, thermal-assistant amorphization leads to the formation of an amorphous phase by a solid-state reaction between the fresh surfaces of Al–Ta interfaces. At the final stage of milling, however, the mechanical-driving force only is responsible for the formation of the amorphous phase.

(4) The amorphous phase existing at the early stage of milling occurs mainly as a result of solid-state diffusion. In the intermediate stage of milling the formation of the amorphous phase occurs as a result of the rod-milling of the alloy powders.

(5) The amorphization process of Al_xTa_{1-x} alloy powders in the Al-rich alloy powders ($x=0.67$) occurs slowly. However, in the Ta-rich powders ($x=0.50$, 0.33) the amorphization process occurs quickly.

(6) The rate of amorphization depends on the tantalum content of the alloy powders. The rate of amorphization increases with increasing tantalum content.

(7) The amorphous Al_xTa_{1-x} ($x=0.67$, 0.50 and 0.33) alloy powders crystallize through a single sharp peak.

(8) The Avrami exponent, n, of the milled Al_xTa_{1-x} alloy powders for 2880 ks, has been calculated to be 1.75, 1.11 and 0.34 for $x=0.67$, 0.50 and 0.33 respectively.

Acknowledgments

This work was partially supported by Ministry of Education, Science and Culture, Grant-in-Aid for Developmental Scientific Research (B) 03555139 and Grant-in-Aid for Co-operative Research (03302053).

References

1 R. B. Schwarz and W. L. Johnson, *Phys. Rev. Lett.*, *51* (1983) 415.
2 C. C. Koch, O. B. Cavin, C. G. Makamey and J. O. Scarbourgh, *Appl. Phys. Lett.*, *43* (1983) 1017.
3 M. Sherif El-Eskandarany, F. Itoh, K. Aoki and K. Suzuki, *J. Non-Cryst. Solids*, *117–118* (1990) 729.
4 M. Sherif El-Eskandarany, K. Aoki, H. Itoh and K. Suzuki, *J. Less-Common Met.*, *169* (1991) 235.
5 M. Sherif El-Eskandarany, K. Sumiyama, K. Aoki and K. Suzuki, in P. H. Shingu (ed.), *Proc. Int. Symp. Mech. Alloying (ISMA), Kyoto, Japan, May 7–10, 1991, Mater. Sci. Forum, 88–90* (1992) 801.
6 M. Sherif El-Eskandarany, K. Sumiyama, K. Aoki and K. Suzuki, *J. Mater. Res.*, in the press.
7 M. Sherif El-Eskandarany, K. Aoki and K. Suzuki, *J. Less-Common Met.*, *167* (1990) 113.
8 M. Sherif El-Eskandarany, H. Suzuki, K. Aoki and K. Suzuki, *J. Jpn. Soc. Powder and Powder Metall.*, *38*(7) (1991) 934.
9 M. Sherif El-Eskandarany, K. Aoki and K. Suzuki, *J. Jpn. Soc. Powder and Powder Metall.*, *38*(1) (1991) 59.
10 M. Sherif El-Eskandarany, K. Aoki and K. Suzuki, *J. Alloys Comp.*, *169* (1991) 235.
11 M. Sherif El-Eskandarany, K. Aoki and K. Suzuki, *Scr. Metall.*, *25* (1991) 1695.
12 M. Sherif El-Eskandarany, K. Aoki and K. Suzuki, *J. Met. Trans.* A, in the press.
13 M. Sherif El-Eskandarany, K. Aoki and K. Suzuki, *J. Appl. Phys.*, *71* (1992) 2924.
14 M. Sherif El-Eskandarany, K. Aoki and K. Suzuki, in P. Shingu (ed.), *Proc. Int. Symp. Mech. Alloying ISMA, Kyoto, Japan, May 7–10, 1991, Mater. Sci. Forum, 88–90* (1992) 81.
15 H. E. Kissinger, *Anal. Chem.*, *29* (1957) 1702.
16 W. A. Johnson and R. F. Mehl, *Trans. AIME*, *135* (1939) 416.
17 M. Avrami, *J. Chem. Phys.*, *9* (1941) 177.